Picosecond Spin Current Generation from Vicinal Metal-Antiferromagnetic Insulator Interfaces

B. Yang,[1,‡] Qing Ji,[1,‡] F. Z. Huang,[1,‡] Jiacong Li,[1] Y. Z. Tian,[1] B. Xue,[1] Ruxian Zhu,[1] Hui Wu,[1] Hanyue Yang,[1] Y. B. Yang,[1] Shaolong Tang,[1] H. B. Zhao,[2] Y. Cao,[1] J. Du,[1] B. G. Wang,[1] Chunfeng Zhang,[1,*] and D. Wu[1,†]

[1]*National Laboratory of Solid State Microstructures, Jiangsu Provincial Key Laboratory for Nanotechnology, Collaborative Innovation Center of Advanced Microstructures and Department of Physics, Nanjing University, Nanjing 210093, People's Republic of China*

[2]*Key Laboratory of Micro and Nano Photonic Structures (Ministry of Education), Department of Optical Science and Engineering, Fudan University, Shanghai 200433, People's Republic of China*

(Received 6 October 2023; accepted 22 March 2024; published 25 April 2024)

We report the picosecond spin current generation from the interface between a heavy metal and a vicinal antiferromagnet insulator Cr_2O_3 by laser pulses at room temperature and zero magnetic field. It is converted into a detectable terahertz emission in the heavy metal via the inverse spin Hall effect. The vicinal interfaces are apparently the source of the picosecond spin current, as evidenced by the proportional terahertz signals to the vicinal angle. We attribute the origin of the spin current to the transient magnetic moment generated by an interfacial nonlinear magnetic-dipole difference-frequency generation. We propose a model based on the in-plane inversion symmetry breaking to quantitatively explain the terahertz intensity with respect to the angles of the laser polarization and the film azimuth. Our work opens new opportunities in antiferromagnetic and ultrafast spintronics by considering symmetry breaking.

DOI: 10.1103/PhysRevLett.132.176703

Antiferromagnets (AFMs) exhibit promising advantages and great potential in spintronic applications due to their unique properties, including ultrafast spin dynamics and zero (or negligible) magnetic moment. These characteristics make AFMs a promising platform for developing devices with ultrafast information processing speed, robustness against external magnetic field perturbations, and high density [1–7]. Spin currents play a crucial role in transporting and manipulating information in spintronic devices [8–13]. In the past few years, much research has focused on exploring static spin current generated from AFMs, such as the spin Seebeck effect (SSE) [14–16] and spin pumping [17–19]. These mechanisms are similar to those observed in ferromagnets. However, the requirement of a strong magnetic field in these effects severely impedes their exploitations and applications [6]. Moreover, the static spin currents generated from AFMs are not fundamentally different from those generated from ferromagnets.

Ultrafast spin currents are an essential ingredient for high-speed spintronic devices [6,7,20–25]. It is anticipated that AFMs can play to their strength of ultrafast spin dynamics on the picosecond timescale to produce picosecond spin currents. However, ferromagnets have been more used as the sources of the picosecond spin currents in two ways with femtosecond laser excitation: the spin-dependent superdiffusive transport of nonequilibrium hot electrons [21–27] and the picosecond SSE [20,28–32], although the spin dynamics of ferromagnets is on the nanosecond timescale [33–35]. In addition, the conversion of picosecond spin currents from pulse electrical currents in a heavy metal (HM) via the spin Hall effect (SHE) has been demonstrated [36]. Until recently, two distinctive mechanisms for optically generated picosecond spin currents in AFMs are discovered in Pt/NiO bilayers. One is the stimulated Raman-induced collinear difference-frequency generation (DFG) optical process [6,37]. This process is permitted only when laser pulses propagate along the threefold symmetry axis of the single crystalline NiO film [38]. The other one is the spin-phonon interactions [7], where the laser-pulse-excited strain waves in Pt modulate the magnetic anisotropy of NiO, inducing Néel vector oscillations and exciting transient antiferromagnetic magnons. The presence of an out-of-plane Néel vector component is required for this mechanism. Additionally, the picosecond SSE has been demonstrated to generate ultrafast spin currents in HM/AFM bilayers with applying large magnetic field [39]. In all previous reports, the bulk properties of ferromagnets, HMs or AFMs have predominantly influenced the generation of picosecond spin currents and it needs to be specific crystal orientation or large magnetic field for AFMs.

The transient magnetic moment, accompanied by the change of the angular momentum over time, can generate a short pulse spin current [40]. Nonlinear magnetic-dipole (MD) transitions can be utilized as an optical method to excite transient magnetic moment in the terahertz (THz) frequency [6,38]. While nonlinear electric-dipole transitions at vicinal surfaces or interfaces have been intensively

studied in nonlinear optics [41,42], it remains unexplored whether the nonlinear MD transition at vicinal metal-AFM interfaces can excite transient magnetic moments and resultant spin current due to the breaking of space- and time- inversion symmetry. In this work, we show the generation of picosecond spin currents using a femtosecond pulse laser in HM/Cr_2O_3 bilayers grown on a vicinal substrate at room temperature and zero magnetic field. The picosecond spin current is converted into a transient charge current in the HM layer via the inverse spin Hall effect (ISHE) [43], resulting in detectable electromagnetic emissions with THz frequencies. The intensity of the THz signal is found to be proportional to the vicinal angle and negligible for the flat film, manifesting that the picosecond spin current is solely contributed from the step edges. We propose an interfacial MD DFG to excite transient magnet moments or magnons as the origin of the picosecond spin current. This finding opens a new avenue for optically generating ultrafast spin current from interface states, in sharp contrast to the existing approaches primarily based on bulk properties.

We choose one-side-polished vicinal $Al_2O_3(0001)$ substrates with steps parallel to the $[10\bar{1}0]$ direction to epitaxially grow Cr_2O_3 films using pulsed laser deposition. The substrates were annealed at 1000 °C for 4 h in air to obtain stepped surfaces. Figure 1(a) shows a typical atomic force microscopy (AFM) image of an $Al_2O_3(0001)$ substrate, clearly displaying the step morphology with straight step edges and uniformly flat terraces, the averaging ~54 nm in width. The height profile as marked by the white line in Fig. 1(a) shows that the step edges have an almost equal height of ~0.44 nm, corresponding to one-third of the lattice constant along the Al_2O_3 [0001] axis [44]. The estimated vicinal angle α of 0.5°, derived from the terrace width and step height, is consistent with the nominal value. Subsequently, the Cr_2O_3 films were grown at 700 °C in an oxygen atmosphere of 0.07 torr with a KrF excimer laser at a repetition of 4 Hz with an energy density of 50 mJ/mm^2. The structure of the Cr_2O_3 films was characterized by *in situ* reflection high energy electron diffraction and x-ray diffraction (see Supplemental Material [45]). The surface displays cracks due to the lattice mismatch between Cr_2O_3 and Al_2O_3 [Fig. 1(b)], but it remains a steplike surface. The vicinal angle α of the film is estimated to be ~0.5° from the height profile [Fig. 1(b)], consistent with that of the substrate. The metallic films were directly deposited onto Cr_2O_3 using dc magnetron sputtering at ambient temperature.

Figure 1(c) illustrates the time-domain THz measurement configuration to demonstrate the laser-stimulated picosecond spin currents. A linearly polarized femtosecond laser with temporal duration 290 fs, central wavelength 1030 nm, and repetition rate 50 kHz (Pharos, Light Conversion) is perpendicularly incident to the sample surface. The direction of the laser polarization and the step direction are defined by the angle θ and φ, respectively, with respect to the x' axis of the laboratory coordinates, as shown in Figs. 1(c) and 1(d). A transient spin current excited by the laser pulses flows into the HM layer and is then converted into a transient transverse charge current via ISHE. This charge current generates an electromagnetic wave with THz frequencies. To detect the THz signal, we employ standard electro-optical sampling using a 1-mm-thick GaP crystal in a dry N_2 environment. The emitted THz waveforms are found to be linearly polarized (see Supplemental Material [45]). In the following measurements, the polarization direction of a wire-grid polarizer placed in front of the GaP crystal is fixed along the x' axis to analyze the x' component of the THz electrical field $E_{x'}^{\mathrm{THz}}$. All THz measurements were performed at room temperature.

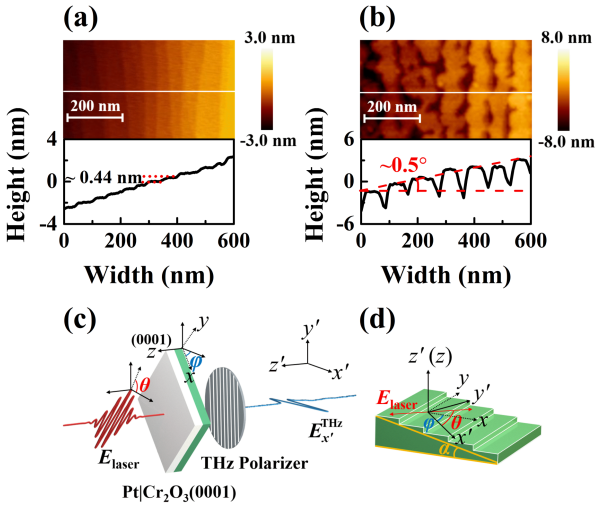

FIG. 1. AFM image and height profile marked by the white line of (a) $Al_2O_3(0001)$ substrate and (b) 15-nm-thick $Cr_2O_3(0001)$ film with $\alpha = 0.5°$. (c) The schematic of the time-domain THz spectroscopy measurement setup. (d) The relation between crystal and laboratory coordinates. The polarization of the laser E_{laser} is defined by the angle θ with respect to x'. The sample surface is set in the $x'y'$ plane and the azimuth angle is defined by φ with respect to x'.

Figure 2(a) shows the temporal evolution of $E_{x'}^{\mathrm{THz}}$ measured on a series of Pt(4)/Cr_2O_3(15) bilayers grown on $Al_2O_3(0001)$ substrates with different α under a laser pump fluence $P = 2.2$ mJ/cm^2 at $\theta = \varphi = 0°$, where the values in parentheses are the thickness in nanometers. The THz emission amplitude is negligible for the sample with $\alpha = 0.1°$, but it rapidly increases with increasing α. The dependence of the peak values, extracted from Fig. 2(a), on α is plotted in Fig. 2(b). The peak values of $E_{x'}^{\mathrm{THz}}$ are linearly dependent on α and approaches zero at $\alpha = 0°$, highlighting the decisive role of the vicinal surface in THz generation. These observations immediately exclude the mechanism discovered in Pt/NiO(111) bilayers where the films are grown on flat substrates [6]. We compare the THz

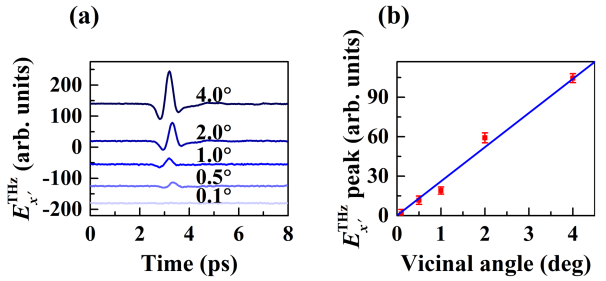

FIG. 2. (a) The time domain spectroscopy of $E_{x'}^{\mathrm{THz}}$ measured on a series of $\mathrm{Pt}(4)/\mathrm{Cr_2O_3}(15)$ bilayers grown on the $\mathrm{Al_2O_3}(0001)$ substrates with different α at $\theta = \varphi = 0°$. (b) The α dependence of the peak values of $E_{x'}^{\mathrm{THz}}$.

emission of $\mathrm{Pt}/\mathrm{Cr_2O_3}$ with those of Pt/NiO, $\mathrm{Pt}/\mathrm{Y_3Fe_5O_{12}}$, and Pt/Py (see Supplemental Material [45]). The amplitude is comparable with those of Pt/NiO and $\mathrm{Pt}/\mathrm{Y_3Fe_5O_{12}}$, but much smaller than that of Pt/Py. The bandwidths of these samples are nearly the same. It is plausibly limited by the time duration of the laser as used in generating and detecting the THz emission, which is the common feature in these measurements. The THz signals of $\mathrm{Pt}/\mathrm{Cr_2O_3}$ are significantly stronger than those of the samples grown on the unannealed substrates with rougher surfaces (see Supplemental Material [45]), again indicating an interfacial origin.

To investigate the origin of the THz emission, we performed several control experiments. First, we fabricated three control samples, $\mathrm{Al}(5)/\mathrm{Cr_2O_3}(15)$ bilayer, Pt(4) single layer, and single $\mathrm{Cr_2O_3}(15)$ film, on vicinal $\mathrm{Al_2O_3}$ substrates with $\alpha = 2°$ to carry out the same measurements. No THz signal is detected in any of the control samples, as shown in Fig. 3(a), where either the Pt or $\mathrm{Cr_2O_3}$ layer is absent. This result highlights the importance of Pt and $\mathrm{Cr_2O_3}$ and excludes the possibility of emission from the $\mathrm{Cr_2O_3}$ layer itself due to the nonlinear optical effects. Second, the THz waveform changes the polarity when W is replaced with Pt on $\mathrm{Cr_2O_3}$ [Fig. 3(a)], indicating the opposite direction of the transient charge current for the W and Pt samples. Considering that W and Pt have opposite spin Hall angles [54], this observation is consistent with the spin current scenario. Furthermore, when considering the negligible THz signal in the $\mathrm{Al}/\mathrm{Cr_2O_3}$ sample, where Al has a very small spin Hall angle [55], we can unambiguously conclude the THz emission arising from the picosecond spin current. Third, the absence of signal in the single Pt film further confirms that our observation is related to antiferromagnet and hence spin current.

Next, we investigated the mechanism of the picosecond spin current generation. $\mathrm{Cr_2O_3}$ is a magnetoelectric AFM material with a corundum type crystal structure, and a bulk Néel temperature of 307.5 K [47,56]. The Néel temperature of our films is measured to be ~360 K, consistent with previous report (see Supplemental Material [45]). The

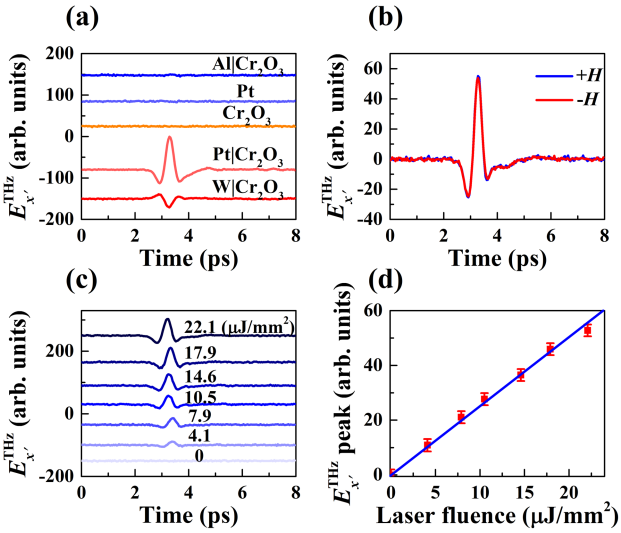

FIG. 3. (a) $E_{x'}^{\mathrm{THz}}$ of $\mathrm{Al}(5)/\mathrm{Cr_2O_3}(15)$, Pt(4), $\mathrm{Cr_2O_3}(15)$, $\mathrm{Pt}(4)/\mathrm{Cr_2O_3}(15)$, and $\mathrm{W}(4)/\mathrm{Cr_2O_3}(15)$ on $\mathrm{Al_2O_3}$ substrates with $\alpha = 2°$ at $\theta = \varphi = 0°$. (b) Response of $E_{x'}^{\mathrm{THz}}$ to external fields of $\mathrm{Pt}(4)/\mathrm{Cr_2O_3}(15)$ with $\alpha = 2°$ at $\theta = \varphi = 0°$. (c) The time domain spectroscopy of $E_{x'}^{\mathrm{THz}}$ measured on $\mathrm{Pt}(4)/\mathrm{Cr_2O_3}(15)$ with different pump laser fluence with $\alpha = 2°$ at $\theta = \varphi = 0°$. (d) The peak values of $E_{x'}^{\mathrm{THz}}$ as a function of the pump fluence, the solid blue line is a linear fit.

temperature of $\mathrm{Cr_2O_3}$ is estimated to increase ~3 K due to the laser heating by a numerical simulation, below the Néel temperature (see Supplemental Material [45]). The Néel vector is along the [0001] direction, perpendicular to the film plane. An uncompensated magnetic moment at the boundary (surface or interface) is present regardless of roughness due to a general symmetry argument [56,57]. This uncompensated magnetic moment could be the source of the picosecond spin current, similar to what is observed in HM/FM bilayers. First, we found that the signals remain almost unchanged when the polarity of an in-plane 1000-Oe external magnetic field is reversed [Fig. 3(b)], inconsistent with the THz signal generated from a ferromagnet. Second, considering that the uncompensated magnetic moment in $\mathrm{Cr_2O_3}$ (0001) is perpendicular to the surface, the THz emission would not be expected from ISHE even if a spin current is excited. Therefore, we can rule out this possibility.

In the optical process, a magnetic moment $\mathbf{M}(\Omega)$ at frequency Ω could be excited through the MD transition even for an AFM without applying a magnetic field:

$$\mathbf{M}(\Omega) \propto \chi^{(1)\mathrm{MD}}\mathbf{E}(\Omega) + \chi^{(2)\mathrm{MD}} : \mathbf{E}(\Omega-\omega)\mathbf{E}(\omega) + \cdots, \quad (1)$$

where $\mathbf{E}(\Omega-\omega)$ and $\mathbf{E}(\omega)$ are the electric fields of the light wave at frequency $\Omega-\omega$ and ω, respectively [58]. The first term on the right-hand side corresponds to the linear magnetoelectric effect with the corresponding linear susceptibility $\chi^{(1)\mathrm{MD}}$. The second term describes the generation of a magnetic moment through a MD DFG process

with the corresponding nonlinear susceptibility $\chi^{(2)\mathrm{MD}}$, which is a third-rank axial tensor. This induced $\mathbf{M}$ could lead to a picosecond SSE owing to the laser pulse excited temperature gradient ∇T, which is proportional to P [29]. According to the SSE mechanism, $E_{x'}^{\mathrm{THz}}$ is determined by

$$E_{x'}^{\mathrm{THz}} \propto J_s \propto \nabla T M \propto PM, \tag{2}$$

where J_s is the amplitude of the spin current. Figure 3(c) presents $E_{x'}^{\mathrm{THz}}$ measured with different P on $\mathrm{Pt}(4)/\mathrm{Cr_2O_3}(15)$ at $\theta = \varphi = 0°$ and $\alpha = 2°$. The peak signals are proportional to P, as shown in Fig. 3(d). It means that $\mathbf{M}$ is independent of P according to Eq. (2), contrary to Eq. (1) that $\mathbf{M}$ is correlated with P or $\mathbf{E}$. Therefore, the SSE mechanism can be excluded to explain our observations.

Owing to the conservation of angular momentum, the variation of $\mathbf{M}$ and its associated angular momentum over time can produce a spin current in the adjacent normal metal, similar to the spin pumping effect. Therefore, the picosecond impulse $\mathbf{M}$ itself can generate the picosecond spin current with its amplitude proportional to $\mathbf{M}$, $M \propto J_s$. Given that $J_s \propto E_{x'}^{\mathrm{THz}} \propto P \propto E^2$ [Fig. 3(d)], we infer that the impulse $\mathbf{M}$ arises solely from the second term of Eq. (1).

The impulse $\mathbf{M}$ and the resulting THz emission can originate from various sources, including the bulk, terraces, and step edges on vicinal interface. Since the bulk properties and the area of the terraces are irrelevant to α, one would expect that the THz emission is independent of α. The negligible THz signal for $\alpha \sim 0°$ [Fig. 2(b)] provides evidence that the contributions from the bulk and the terraces can be omitted. On the other hand, due to the in-plane inversion symmetry breaking at the steps, photons are in a local asymmetric potential field around the step edges. As a result, the nonlinear MD transition occurs only around the step edges [58], meaning that $\mathbf{M}$ is localized around the step edges and the magnitude is proportional to the step height. If the direction of the steps is reversed, the direction of $\mathbf{M}$ is reversed. Therefore, the total $\mathbf{M}$, which is the integral of all moments at the step edges, is approximately proportional to α or the total step height, consistent with the behavior of $E_{x'}^{\mathrm{THz}}$, regardless of the cracks in the films [Fig. 1(b)].

The MD transition contributed from $\chi^{(2)\mathrm{MD}}$ can be classified into time-symmetric (i-type) $\chi^{(i)}$ and time-antisymmetric (c-type) $\chi^{(c)}$ susceptibilities for magnetic materials [59,60], $\chi^{(2)\mathrm{MD}} = \chi^{(i)} + \chi^{(c)}$. The direction of the magnetic moment is reversed by time inversion, which is equivalent to the switching of the antiferromagnetic Néel vector. In our as-grown $\mathrm{Cr_2O_3}(0001)$ films, there are randomly distributed opposite 180° antiferromagnetic domains with $\chi^{(i)}$ of the same sign and $\chi^{(c)}$ of the opposite sign. The THz signals coming from each domain are coherently superposed, resulting in the cancellation of the contribution from $\chi^{(c)}$ and leaving only the contribution from $\chi^{(i)}$.

The magnetic point group of the vicinal $\mathrm{Cr_2O_3}$ surface below the Néel temperature is $\underline{m}$, which consists of two symmetry operators, 1 and $\bar{\underline{2}}_y$ [60]. Here, we use crystal coordinates to describe the components of the susceptibility tensor, as depicted in Fig. 1(d), in which the y axis is along the step edge and the x axis is perpendicular to the step face. For light propagating along the z axis and ISHE in the HM layer depending only on the in-plane magnetic moment $\mathbf{M}_{x-y}$, only three independent nonzero components need to be considered for $\chi^{(i)}$, $\chi_{yxx}^{(i)}$, $\chi_{yyy}^{(i)}$ and $\chi_{xxy}^{(i)} = \chi_{xyx}^{(i)} \equiv \gamma$. The excited $\mathbf{M}_{x-y}$ is then given by

$$\mathbf{M}_{x-y} = \begin{pmatrix} M_x \\ M_y \end{pmatrix} \propto \alpha \begin{pmatrix} 2\gamma E_x E_y \\ \chi_{yxx}^{(i)} E_x^2 + \chi_{yyy}^{(i)} E_y^2 \end{pmatrix}, \tag{3}$$

where it is applied that $\mathbf{M}_{x-y}$ has a linear dependence on α for small α. In our experimental configuration and the laboratory coordinate system, one can calculate the y' component of $\mathbf{M}$, $M_{y'}$, to obtain the THz emission for the laser polarization along the x' axis, i.e., $\theta = 0°$,

$$E_{x'}^{\mathrm{THz}} \propto M_{y'} \propto [(\chi_{yyy}^{(i)} - 2\gamma)\sin^2\varphi + \chi_{yxx}^{(i)}\cos^2\varphi]\alpha P \cos\varphi. \tag{4}$$

When the laser polarization is varied while fixing the sample orientation with $\varphi = 0°$, the THz emission is calculated as

$$E_{x'}^{\mathrm{THz}} \propto M_{y'} \propto [\chi_{yxx}^{(i)} + (\chi_{yyy}^{(i)} - \chi_{yxx}^{(i)})\sin^2\theta]\alpha P. \tag{5}$$

According to Eqs. (4) and (5), the amplitude of the THz emission is proportional to α and P, in good agreement with the experimental results [Figs. 2(b) and 3(d)].

To further validate the above phenomenological model based on symmetrical analysis, we performed angular-dependent measurements. In Figs. 4(a) and 4(c), we present the THz waveforms of the $\mathrm{Pt}(4)/\mathrm{Cr_2O_3}(15)$ bilayers sample with $\alpha = 2°$ for various φ at $\theta = 0°$ and various θ at $\varphi = 0°$, respectively. The corresponding $E_{x'}^{\mathrm{THz}}$ peak values as functions of φ and θ are shown in Figs. 4(b) and 4(d), respectively. These angular dependences could be caused by the change of the laser absorption [61–63]. We find that the laser absorption is independent of θ and hence this impact is excluded (see Supplemental Material [45]). We fitted the data for φ- and θ-scans with Eqs. (4) and (5), respectively. The fittings are in good agreement with the data and yield $\chi_{yxx}^{(i)} : \chi_{yyy}^{(i)} : \chi_{xxy}^{(i)} : \chi_{xyx}^{(i)} \approx 55 : 35 : -12 : -12$. Without considering the symmetry of the $\mathrm{Cr_2O_3}$ lattice, the mirror symmetry is broken about the yz pane due to the steps, but it remains about the xz pane in the vicinal surface. Therefore, the second-order nonlinear optical process should be strongest at the light polarization parallel to the

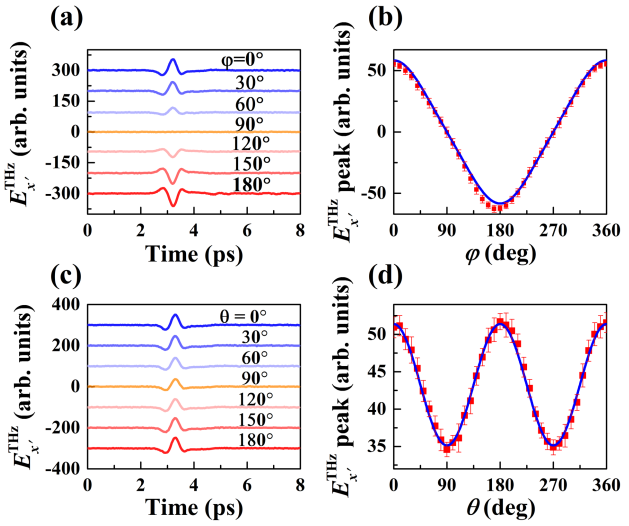

FIG. 4. The THz waveforms of the $Pt(4)/Cr_2O_3(15)$ bilayers with $\alpha = 2°$ for (a) various φ at $\theta = 0$ and (c) various θ at $\varphi = 0°$. The corresponding peak values of $E_{x'}^{\mathrm{THz}}$ as functions of (b) φ and (d) θ. The red dots are the raw data, and the blue lines represent the fitted curves with Eqs. (4) and (5), respectively.

x axis [41]. This is consistent with the strongest signal at $\varphi = 0°$ and 180° in Fig. 4(b) and at $\theta = 0°$ and 180° in Fig. 4(d). Note that rotating the sample by 180° is equivalent to changing the sign of α, resulting the sign reversal of $E_{x'}^{\mathrm{THz}}$. As a result, the THz emission amplitude exhibits an oscillation period of 360° in the φ scan but an oscillation period of 180° in the θ scan. In the φ scan, the threefold symmetry of Cr_2O_3 is not present, again confirming the negligible bulk contribution.

In summary, we show a transient magnetic moment optically excited at the vicinal metal-Cr_2O_3 interface at zero magnetic field and room temperature. This transient magnetic moment is converted into a picosecond spin current. We attribute these observations to the interfacial MD DFG process induced magnetic moment, which originates from the in-plane inversion symmetry breaking at interface. This effect disappears in the flat sample, confirming the sole contribution from the step edges. We observe a clear dependence on laser polarization direction and sample azimuth angle, which is consistent with our theoretical model based on symmetry analysis. Our findings highlight that the MD DFG process can be a general approach to generate ultrafast spin current by considering the symmetries. Our observation is understood by the nonlinear optical process due to the space- and the time-inversion symmetry breaking at the vicinal interfaces. We anticipate that the picosecond spin current generation by this interfacial effect is valid for other HM-AFM or even HM-ferromagnet interfaces. This will open up more opportunities in antiferromagnetic and ultrafast spintronics.

This work was supported by National Key R&D Program of China (2022YFA1403602) and National Natural Science Foundation of China (52025012, 22225305, 12334007, 12374112 and T2394473).

*Corresponding author: cfzhang@nju.edu.cn
†Corresponding author: dwu@nju.edu.cn
‡These authors contributed equally to this work.

[1] V. Baltz, A. Manchon, M. Tsoi, T. Moriyama, T. Ono, and Y. Tserkovnyak, Antiferromagnetic spintronics, Rev. Mod. Phys. **90**, 015005 (2018).
[2] T. Jungwirth, X. Marti, P. Wadley, and J. Wunderlich, Antiferromagnetic spintronics, Nat. Nanotechnol. **11**, 231 (2016).
[3] E. G. Tveten, A. Qaiumzadeh, and A. Brataas, Antiferromagnetic domain wall motion induced by spin waves, Phys. Rev. Lett. **112**, 147204 (2014).
[4] J. Han, R. Cheng, L. Liu, H. Ohno, and S. Fukami, Coherent antiferromagnetic spintronics, Nat. Mater. **22**, 684 (2023).
[5] L. Baldrati, O. Gomonay, A. Ross, M. Filianina, R. Lebrun, R. Ramos, C. Leveille, F. Fuhrmann, T. R. Forrest, F. Maccherozzi, S. Valencia, F. Kronast, E. Saitoh, J. Sinova, and M. Kläui, Mechanism of Néel order switching in antiferromagnetic thin films revealed by magnetotransport and direct imaging, Phys. Rev. Lett. **123**, 177201 (2019).
[6] H. Qiu, L. Zhou, C. Zhang, J. Wu, Y. Tian, S. Cheng, S. Mi, H. Zhao, Q. Zhang, D. Wu, B. Jin, J. Chen, and P. Wu, Ultrafast spin current generated from an antiferromagnet, Nat. Phys. **17**, 388 (2021).
[7] E. Rongione, O. Gueckstock, M. Mattern, O. Gomonay, H. Meer, C. Schmitt, R. Ramos, T. Kikkawa, M. Mičica, E. Saitoh, J. Sinova, H. Jaffrès, J. Mangeney, S. T. B. Goennenwein, S. Geprägs, T. Kampfrath, M. Kläui, M. Bargheer, T. S. Seifert, S. Dhillon, and R. Lebrun, Emission of coherent THz magnons in an antiferromagnetic insulator triggered by ultrafast spin-phonon interactions, Nat. Commun. **14**, 1818 (2023).
[8] I. Žutić, J. Fabian, and S. Das Sarma, Spintronics: Fundamentals and applications, Rev. Mod. Phys. **76**, 323 (2004).
[9] A. Manchon, J. Železný, I. M. Miron, T. Jungwirth, J. Sinova, A. Thiaville, K. Garello, and P. Gambardella, Current-induced spin-orbit torques in ferromagnetic and antiferromagnetic systems, Rev. Mod. Phys. **91**, 035004 (2019).
[10] L. J. Cornelissen, J. Liu, B. J. van Wees, and R. A. Duine, Spin-current-controlled modulation of the magnon spin conductance in a three-terminal magnon transistor, Phys. Rev. Lett. **120**, 097702 (2018).
[11] Q. Ma, Y. Li, D. B. Gopman, Y. P. Kabanov, R. D. Shull, and C. L. Chien, Switching a perpendicular ferromagnetic layer by competing spin currents, Phys. Rev. Lett. **120**, 117703 (2018).
[12] Y. Wang, D. Zhu, Y. Yang, K. Lee, R. Mishra, G. Go, S. H. Oh, D. H. Kim, K. Cai, E. Liu, S. D. Pollard, S. Shi, J. Lee, K. L. Teo, Y. Wu, K. J. Lee, and H. Yang, Magnetization switching by magnon-mediated spin torque through an antiferromagnetic insulator, Science **366**, 1125 (2019).

[13] X. Z. Chen, R. Zarzuela, J. Zhang, C. Song, X. F. Zhou, G. Y. Shi, F. Li, H. A. Zhou, W. J. Jiang, F. Pan, and Y. Tserkovnyak, Antidamping-torque-induced switching in biaxial antiferromagnetic insulators, Phys. Rev. Lett. **120**, 207204 (2018).

[14] S. Seki, T. Ideue, M. Kubota, Y. Kozuka, R. Takagi, M. Nakamura, Y. Kaneko, M. Kawasaki, and Y. Tokura, Thermal generation of spin current in an antiferromagnet, Phys. Rev. Lett. **115**, 266601 (2015).

[15] S. M. Wu, W. Zhang, A. KC, P. Borisov, J. E. Pearson, J. S. Jiang, D. Lederman, A. Hoffmann, and A. Bhattacharya, Antiferromagnetic spin Seebeck effect, Phys. Rev. Lett. **116**, 097204 (2016).

[16] J. Li, Z. Shi, V. H. Ortiz, M. Aldosary, C. Chen, V. Aji, P. Wei, and J. Shi, Spin Seebeck effect from antiferromagnetic magnons and critical spin fluctuations in epitaxial FeF_2 films, Phys. Rev. Lett. **122**, 217204 (2019).

[17] P. Vaidya, S. A. Morley, J. van Tol, Y. Liu, R. Cheng, A. Brataas, D. Ledermanand, and E. del Barco, Subterahertz spin pumping from an insulating antiferromagnet, Science **368**, 160 (2020).

[18] J. Li, C. B. Wilson, R. Cheng, M. Lohmann, M. Kavand, W. Yuan, M. Aldosary, N. Agladze, P. Wei, M. S. Sherwin, and J. Shi, Spin current from sub-terahertz-generated antiferromagnetic magnons, Nature (London) **578**, 7793 (2020).

[19] H. Wang, Y. Xiao, M. Guo, E. Lee-Wong, G. Q. Yan, R. Cheng, and C. R. Du, Spin pumping of an easy-plane antiferromagnet enhanced by Dzyaloshinskii-Moriya interaction, Phys. Rev. Lett. **127**, 117202 (2021).

[20] P. Jiménez-Cavero, O. Gueckstock, L. Nádvorník, I. Lucas, T. S. Seifert, M. Wolf, R. Rouzegar, P. W. Brouwer, S. Becker, G. Jakob, M. Kläui, C. Guo, C. Wan, X. Han, Z. Jin, H. Zhao, D. Wu, L. Morellón, and T. Kampfrath, Transition of laser-induced terahertz spin currents from torque-to conduction-electron-mediated transport, Phys. Rev. B **105**, 184408 (2022).

[21] A. Alekhin, I. Razdolski, N. Ilin, J. P. Meyburg, D. Diesing, V. Roddatis, I. Rungger, M. Stamenova, S. Sanvito, U. Bovensiepen, and A. Melnikov, Femtosecond spin current pulses generated by the nonthermal spin-dependent Seebeck effect and interacting with ferromagnets in spin valves, Phys. Rev. Lett. **119**, 017202 (2017).

[22] C. Zhou, Y. P. Liu, Z. Wang, S. J. Ma, M. W. Jia, R. Q. Wu, L. Zhou, W. Zhang, M. K. Liu, Y. Z. Wu, and J. Qi, Broadband terahertz generation via the interface inverse Rashba-Edelstein effect, Phys. Rev. Lett. **121**, 086801 (2018).

[23] T. Kampfrath, M. Battiato, P. Maldonado, G. Eilers, J. Nötzold, S. Mährlein, V. Zbarsky, F. Freimuth, Y. Mokrousov, S. Blügel, M. Wolf, I. Radu, P. M. Oppeneer, and M. Münzenberg, Terahertz spin current pulses controlled by magnetic heterostructures, Nat. Nanotechnol. **8**, 256 (2013).

[24] Y. S. Liu, H. Y. Cheng, Y. Xu, P. Vallobra, S. Eimer, X. Q. Zhang, X. J. Wu, T. X. Nie, and W. S. Zhao, Separation of emission mechanisms in spintronic terahertz emitters, Phys. Rev. B **104**, 064419 (2021).

[25] C. Q. Liu, W. T. Lu, Z. X. Wei, Y. F. Miao, P. Wang, H. Xia, Y. P. Liu, F. L. Zeng, J. R. Zhang, C. Zhou, H. B. Zhao, Y. Z. Wu, Z. Yuan, and J. Qi, Strain-induced anisotropic terahertz emission from a Fe(211)/Pt(110) bilayer, Phys. Rev. Appl. **15**, 044022 (2021).

[26] M. Battiato, K. Carva, and P. M. Oppeneer, Superdiffusive spin transport as a mechanism of ultrafast demagnetization, Phys. Rev. Lett. **105**, 027203 (2010).

[27] A. Eschenlohr, M. Battiato, P. Maldonado, N. Pontius, T. Kachel, K. Holldack, R. Mitzner, A. Föhlisch, P. M. Oppeneer, and C. Stamm, Ultrafast spin transport as key to femtosecond demagnetization, Nat. Mater. **12**, 332 (2013).

[28] J. Kimling, G.-M. Choi, J. T. Brangham, T. Matalla-Wagner, T. Huebner, T. Kuschel, F. Yang, and D. G. Cahill, Picosecond spin Seebeck effect, Phys. Rev. Lett. **118**, 057201 (2017).

[29] T. S. Seifert, S. Jaiswal, J. Barker, S. T. Weber, I. Razdolski, J. Cramer, O. Gueckstock, S. F. Maehrlein, L. Nadvornik, S. Watanabe, C. Ciccarelli, A. Melnikov, G. Jakob, M. Münzenberg, S. T. B. Goennenwein, G. Woltersdorf, B. Rethfeld, P. W. Brouwer, M. Wolf, M. Kläui, and T. Kampfrath, Femtosecond formation dynamics of the spin Seebeck effect revealed by terahertz spectroscopy, Nat. Commun. **9**, 2899 (2018).

[30] V. H. Ortiz, M. J. Gomez, Y. Liu, M. Aldosary, J. Shi, and R. B. Wilson, Ultrafast measurements of the interfacial spin Seebeck effect in Au and rare-earth iron-garnet bilayers, Phys. Rev. Mater. **5**, 074401 (2021).

[31] F. N. Kholid, D. Hamara, M. Terschanski, F. Mertens, D. Bossini, M. Cinchetti, L. McKenzie-Sell, J. Patchett, D. Petit, R. Cowburn, J. Robinson, J. Barker, and C. Ciccarelli, Temperature dependence of the picosecond spin Seebeck effect, Appl. Phys. Lett. **119**, 32401 (2021).

[32] J. Cramer, T. Seifert, A. Kronenberg, F. Fuhrmann, G. Jakob, M. Jourdan, T. Kampfrath, and M. Kläui, Complex terahertz and direct current inverse spin Hall effect in $YIG/Cu_{1-x}Ir_x$ bilayers across a wide concentration range, Nano Lett. **18**, 1064 (2018).

[33] J. Li, L. R. Shelford, P. Shafer, A. Tan, J. X. Deng, P. S. Keatley, C. Hwang, E. Arenholz, G. Van Der Laan, R. J. Hicken, and Z. Q. Qiu, Direct detection of pure ac spin current by x-ray pump-probe measurements, Phys. Rev. Lett. **117**, 076602 (2016).

[34] Q. Li, M. Yang, C. Klewe, P. Shafer, A. T. N'Diaye, D. Hou, T. Y. Wang, N. Gao, E. Saitoh, C. Hwang, R. J. Hicken, J. Li, E. Arenholz, and Z. Q. Qiu, Coherent ac spin current transmission across an antiferromagnetic CoO insulator, Nat. Commun. **10**, 5265 (2019).

[35] M. Dąbrowski, T. Nakano, D. M. Burn, A. Frisk, D. G. Newman, C. Klewe, Q. Li, M. Yang, P. Shafer, E. Arenholz, T. Hesjedal, G. van der Laan, Z. Q. Qiu, and R. J. Hicken, Coherent transfer of spin angular momentum by evanescent spin waves within antiferromagnetic NiO, Phys. Rev. Lett. **124**, 217201 (2020).

[36] K. Jhuria, J. Hohlfeld, A. Pattabi, E. Martin, A. Y. Arriola Córdova, X. Shi, R. Lo Conte, S. Petit-Watelot, J. C. Rojas-Sanchez, G. Malinowski, S. Mangin, A. Lemaître, M. Hehn, J. Bokor, R. B. Wilson, and J. Gorchon, Spin-orbit torque switching of a ferromagnet with picosecond electrical pulses, National electronics review **3**, 680 (2020).

[37] R. Agarwal, S. Kumar, N. Chowdhury, K. I. A. Khan, E. Yadav, S. Kumar, and P. K. Muduli, Strong impact of crystalline twins on the amplitude and azimuthal dependence of THz emission from epitaxial NiO/Pt, Appl. Phys. Lett. **122**, 082403 (2023).

[38] T. Higuchi, N. Kanda, H. Tamaru, and M. Kuwata-Gonokami, Selection rules for light-induced magnetization of a crystal with threefold symmetry: The case of antiferromagnetic NiO, Phys. Rev. Lett. **106**, 047401 (2011).
[39] F. N. Kholid, D. Hamara, A. F. Bin Hamdan, G. N. Antonio, R. Bowen, D. Petit, R. Cowburn, R. V. Pisarev, D. Bossini, J. Barker, and C. Ciccarelli, The importance of the interface for picosecond spin pumping in antiferromagnet-heavy metal heterostructures, Nat. Commun. **14**, 538 (2023).
[40] L. Bocklage, Coherent THz transient spin currents by spin pumping, Phys. Rev. Lett. **118**, 257202 (2017).
[41] S. Janz, D. J. Bottomley, H. M. van Driel, and R. S. Timsit, Influence of steps on second-harmonic generation from vicinal metal surfaces, Phys. Rev. Lett. **66**, 1201 (1991).
[42] C. W. van Hasselt, M. A. Verheijen, and Th. Rasing, Vicinal Si(111) surfaces studied by optical second-harmonic generation: Step-induced anisotropy and surface-bulk discrimination, Phys. Rev. B **42**, 9263 (1990).
[43] T. Kimura, Y. Otani, T. Sato, S. Takahashi, and S. Maekawa, Room-temperature reversible spin Hall effect, Phys. Rev. Lett. **98**, 156601 (2007).
[44] R. Verre, R. G. S. Sofin, V. Usov, K. Fleischer, D. Fox, G. Behan, H. Zhang, and I. V. Shvets, Equilibrium faceting formation in vicinal $Al_2O_3(0001)$ surface caused by annealing, Surf. Sci. **606**, 1815 (2012).
[45] See Supplemental Material at http://link.aps.org/supplemental/10.1103/PhysRevLett.132.176703 for characteristics of $Cr_2O_3(0001)$ film, polarization state of the THz emission from Cr_2O_3Pt, comparison of the THz emission between Pt/Cr_2O_3 and other systems, the influence of the step quality on the THz signal, estimation of the Néel temperature of $Cr_2O_3(0001)$ films, estimation of the temperature in Cr_2O_3 with laser irradiation, and the laser absorption of Pt/Cr_2O_3. Supplemental Material includes Refs. [46–53].
[46] Y. Cheng, S. S. Yu, M. L. Zhu, J. Hwang, and F. Y. Yang, Evidence of the topological Hall effect in Pt/antiferromagnetic insulator bilayers, Phys. Rev. Lett. **123**, 237206 (2019).
[47] P. Makushko, T. Kosub, O. V. Pylypovskyi, N. Hedrich, J. Li, A. Pashkin, S. Avdoshenko, R. Hübner, F. Ganss, D. Wolf, A. Lubk, M. O. Liedke, M. Butterling, A. Wagner, K. Wagner, B. J. Shields, P. Lehmann, I. Veremchuk, J. Fassbender, P. Maletinsky, and D. Makarov, Flexomagnetism and vertically graded Néel temperature of antiferromagnetic Cr_2O_3 thin films, Nat. Commun. **13**, 6745 (2022).
[48] Z. Feng, W. Tan, Z. Jin, Y.-J. Chen, Z. Zhong, L. Zhang, S. Sun, J. Tang, Y. Jiang, P.-H. Wu, J. Cheng, B. Miao, H. Ding, D. Wang, Y. Zhu, L. Guo, S. Shin, G.-H. Ma, D. Hou, and S.-Y. Huang, Anomalous Nernst effect induced terahertz emission in a single ferromagnetic film, Nano Lett. **23**, 8171 (2023).
[49] G. M. Choi, R. B. Wilson, and D. G. Cahill, Indirect heating of Pt by short-pulse laser irradiation of Au in a nanoscale Pt/Au bilayer, Phys. Rev. B **89**, 064307 (2014).
[50] S. Klemme, H. S. C. O'Neill, W. Schnelle, and E. Gmelin, The heat capacity of $MgCr_2O_4$, $FeCr_2O_4$ and Cr_2O_3 at low temperatures and derived thermodynamic properties, Am. Mineral. **85**, 1686 (2000).
[51] R. K. Williams, R. S. Graves, and D. L. McElroy, Thermal conductivity of Cr_2O_3 in the vicinity of the Neel transition, J. Am. Ceram. Soc. **61**, CIS1 (1984).
[52] H. Zhang, Z. Feng, G. Li, L. Zhang, X. Chen, H. Bai, S. Sun, J. Tang, J. Zhang, F. Han, H. Yang, W. Tan, Y. Chen, F. Hu, J. Cai, L. Guo, S. Shin, W. Zhao, B. Shen, and J. Sun, Tuning terahertz emission generated by anomalous Nernst effect in ferromagnetic metal, Appl. Phys. Rev. **10**, 021417 (2023).
[53] A. P. Caffrey, P. E. Hopkins, J. M. Klopf, and P. M. Norris, Thin film non-noble transition metal thermophysical properties, Microscale Thermophys. Eng. **9**, 365 (2005).
[54] D. Qu, S. Y. Huang, and C. L. Chien, Inverse spin Hall effect in Cr: Independence of antiferromagnetic ordering, Phys. Rev. B **92**, 020418(R) (2015).
[55] J. Sinova, S. O. Valenzuela, J. Wunderlich, C. H. Back, and T. Jungwirth, Spin Hall effects, Rev. Mod. Phys. **87**, 1213 (2015).
[56] X. He, Y. Wang, N. Wu, A. N. Caruso, E. Vescovo, K. D. Belashchenko, P. A. Dowben, and C. Binek, Robust isothermal electric control of exchange bias at room temperature, Nat. Mater. **9**, 579 (2010).
[57] K. D. Belashchenko, Equilibrium magnetization at the boundary of a magnetoelectric antiferromagnet, Phys. Rev. Lett. **105**, 147204 (2010).
[58] M. Fiebig, V. V. Pavlov, and R. V. Pisarev, Second-harmonic generation as a tool for studying electronic and magnetic structures of crystals: Review, J. Opt. Soc. Am. B **22**, 96 (2005).
[59] M. Fiebig, D. Fröhlich, B. B. Krichevtsov, and R. V. Pisarev, Second harmonic generation and magnetic-dipole-electric-dipole interference in antiferromagnetic Cr_2O_3, Phys. Rev. Lett. **73**, 2127 (1994).
[60] P. R. Birss, in Symmetry and Magnetism, *Selected Topics in Solid State Physics Vol. III*, edited by E. P. Wohlfarth (North-Holland, Amsterdam, 1966).
[61] T. Seifert, S. Jaiswal, U. Martens, J. Hannegan, L. Braun, P. Maldonado, F. Freimuth, A. Kronenberg, J. Henrizi, I. Radu, E. Beaurepaire, Y. Mokrousov, P. M. Oppeneer, M. Jourdan, G. Jakob, D. Turchinovich, L. M. Hayden, M. Wolf, M. Münzenberg, M. Kläui, and T. Kampfrath, Efficient metallic spintronic emitters of ultrabroadband terahertz radiation, Nat. Photonics **10**, 483 (2016).
[62] Z. Feng, R. Yu, Y. Zhou, H. Lu, W. Tan, H. Deng, Q. Liu, Z. Zhai, L. Zhu, J. Cai, B. Miao, and H. Ding, Highly efficient spintronic terahertz emitter enabled by metal–dielectric photonic crystal, Adv. Opt. Mater. **6**, 1800965 (2018).
[63] G. Torosyan, S. Keller, L. Scheuer, R. Beigang, and E. T. Papaioannou, Optimized spintronic terahertz emitters based on epitaxial grown Fe/Pt layer structures, Sci. Rep. **8**, 1311 (2018).